Electronic Supplementary Material (ESI) for Journal of Materials Chemistry A.

Supporting Information

Scalable Al-Ni Alloy Powder Catalyst Prepared by Metallurgical Microstructure Control

Sang Won Im,[†a] Hehsang Ahn,[†a] Da Hye Seo,[†a] Sunghak Park,[a] Seungwoo Choi,[a] Wookha Ryu,[a] Kyungjun Kim,[a] Eun Soo Park*[a] and Ki Tae Nam*[a]

[a] Department of Materials Science and Engineering, Seoul National University, Seoul 08826, Korea

[†] These authors contributed equally to this work

* Correspondence to: espark@snu.ac.kr, nkitae@snu.ac.kr

Experimental methods

Sample preparation

$Al_{100-x}Ni_x$ (x = 5, 10, 15, 20, 25) alloy ingots were produced by arc-melting high purity (>99.9%) elements of Al and Ni under a Ti-gettered argon atmosphere in a water-cooled copper crucible. The alloy ingots were re-melted more than five times to improve the compositional homogeneity, then suction casted into a water-cooled copper mold with 2 x 6 x 30 mm rectangular cavity. Alloy specimens were cut into smaller pieces with 10 mm length using grinder. The surfaces of prepared Al-Ni alloy specimens were polished using sandpapers with grit number of 800, 1200, and 2000 in sequence. To selectively etch the aluminum from Al-Ni alloy, pristine specimens were immersed into a 6M KOH solution at room temperature for 12 hours, until no obvious bubbles were produced. During the reaction, the color was changed from metallic white to matte brownish-black. Dealloyed Al-Ni catalysts were rinsed with deionized water and methanol in sequence to remove residual KOH solution and trapped gas bubbles in the dealloyed Al-Ni specimens, and then dried under room temperature.

Structural characterization

Phase identification of the samples was conducted by X-ray diffraction (XRD) on a D8 advance X-ray diffractometer (Bruker Miller Co., Germany) with Cu Kα radiation (λ = 1.5418 Å). Dealloyed Al-Ni alloy samples were ground to powder before placed on a holder. The microstructure of the samples was characterized with Field-Emission Scanning Electron Microscope (SUPRA 55VP, Carl Zeiss, Germany) at an accelerating voltage of 2 kV. Pristine Al-Ni alloy samples were polished using 0.1, 0.05 and 0.01 mm size alumina particles in sequence. The microstructures of alloys were observed in back-scattered electron (BSE) mode. Microstructures of dealloyed Al-Ni alloy samples were observed in secondary electron (SE) mode.

Preparation of dealloyed Al-Ni catalyst electrode

Dealloyed Al-Ni alloys were prepared as electrodes by attaching to Ni foil substrates. Before using, a Ni foil was cleaned by a chemical treatment, immersed in aqueous solutions of 10% volume fraction of hydrochloric acid (HCl) for 1 min at 65 °C. After the cleaning

procedure, the Ni foil was rinsed with deionized water. The dealloyed Al-Ni alloy was attached on the Ni foil by using a silver conductive epoxy (Epoxy Technology, Epo-Tek H70E). Exposed substrate and side area of the catalyst was masked with an epoxy (Loctite, Hysol EA 9460) to define the catalytic surface area and exclude the contribution of electrochemical reaction on Ni foil.

Preparation of dealloyed Al-Ni powder coating electrode

Dealloyed $Al_{90}Ni_{10}$ alloy catalyst was ground to fine powder by a mortar. The ink was prepared by mixing dealloyed Al-Ni powder, activated carbon, polyvinylidene fluoride (PVDF), and N-Methyl-2-pyrrolidone (NMP). Herein, PVDF was used as a polymer binder and NMP was used as a solvent. The mass ratio of activated carbon, PVDF and NMP in the ink was 1: 1: 25. Prepared ink was coated on a Ni foil by controlling the loading amount of catalyst per unit area to be 2 mg cm^{-2}, 5 mg cm^{-2}, 10 mg cm^{-2}, and 25 mg cm^{-2}. Before coating, the Ni foil substrate was roughened with a sandpaper (grit number 100) to improve adhesion. Prepared electrode was cut into pieces with geometric surface area of the catalyst to be 1 cm^2 for electrochemical measurements.

Electrochemical measurements

All electrochemical experiments were conducted in a three-electrode system. Hg/HgO reference electrode (1.0 M KOH, ALS Co., Ltd) and Pt foil counter electrode was used. The inner solution of Hg/HgO reference electrode was exchanged with freshly prepared 1.0 M KOH 24 hours before the experiments. Electrochemical tests were carried out at room temperature using a potentiostat (VSP-300, Bio-Logic Science Instruments) in a 1.0 M KOH solution. The electrode potential versus Hg/HgO was converted to the RHE scale, using the following equation: E(RHE) = E(Hg/HgO) + 0.928 V. Additionally, overpotential was calculated by the difference between the iR-corrected potential ($V = V_{applied} - iR$) and thermodynamic potential of the hydrogen evolving reaction. Chronoamperometric measurements were performed for dealloyed Al-Ni catalyst electrode at each applied potential and the steady-state current density was measured minimizing the contribution of charging current. The powder coating electrode was measured by cyclic voltammetry with scan rate of 1 mV s^{-1}. During the analysis, the electrolyte was stirred by a magnetic bar to remove the hydrogen bubbles on the surfaces of

the electrode.

(a)

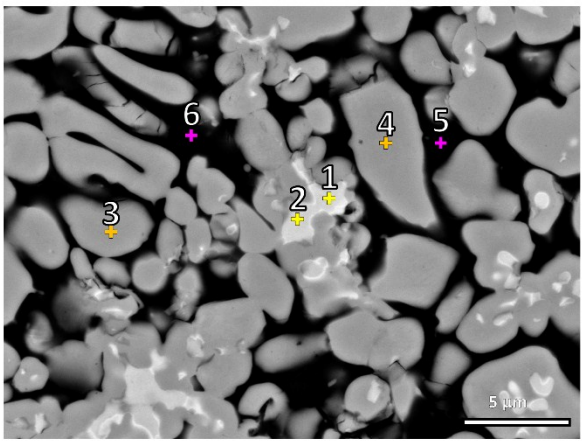

at%		Al	Ni
Al_3Ni_2 phase	1	63.76	36.24
	2	60.92	39.08
Average		**62.34**	**37.66**
Al_3Ni phase	3	75.34	24.66
	4	74.18	25.82
Average		**74.76**	**25.24**
Eutectic phase	5	96.74	3.26
	6	95.09	4.91
Average		**95.91**	**4.09**

(b)

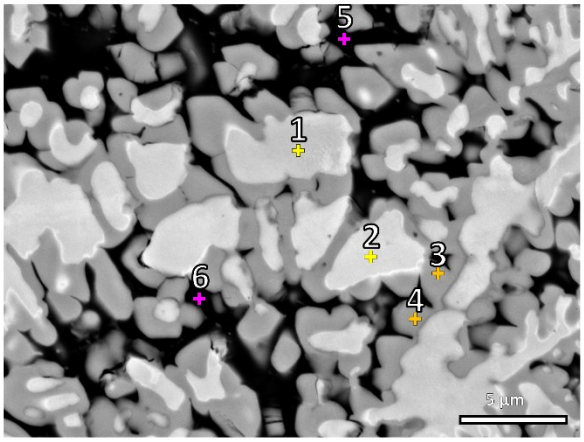

at%		Al	Ni
Al_3Ni_2 phase	1	59.06	40.94
	2	57.49	42.51
Average		**58.28**	**41.72**
Al_3Ni phase	3	73.46	26.54
	4	75.94	24.06
Average		**74.70**	**25.30**
Eutectic phase	5	96.58	3.42
	6	92.95	7.05
Average		**94.77**	**5.23**

Figure S1. BSE image and EDS results of (a) $Al_{80}Ni_{20}$ and (b) $Al_{75}Ni_{25}$ alloy. Position 1 and 2 indicate white Al_3Ni_2 phase, position 3 and 4 indicate bright gray Al_3Ni phase, and position 5 and 6 indicate dark gray eutectic phase. Average values of the composition from each phase are shown in the tables.

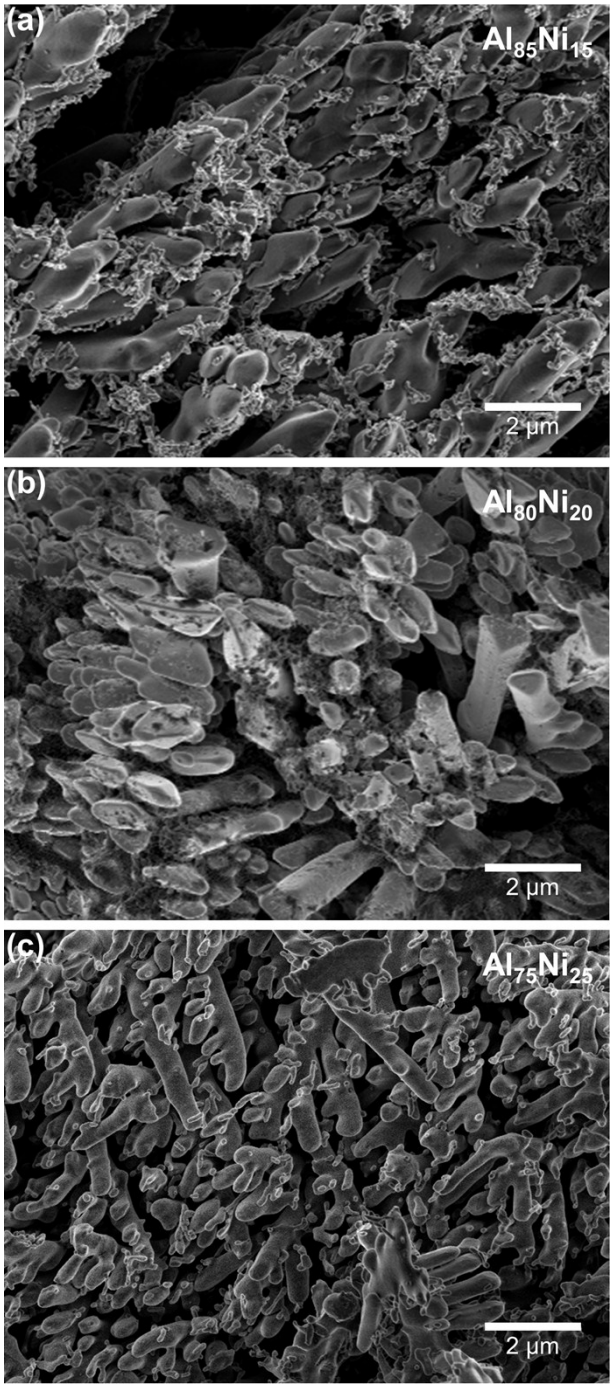

Figure S2. Scanning electron microscopy image of (a) $Al_{85}Ni_{15}$, (b) $Al_{80}Ni_{20}$, and (c) $Al_{80}Ni_{20}$ alloys after etching.

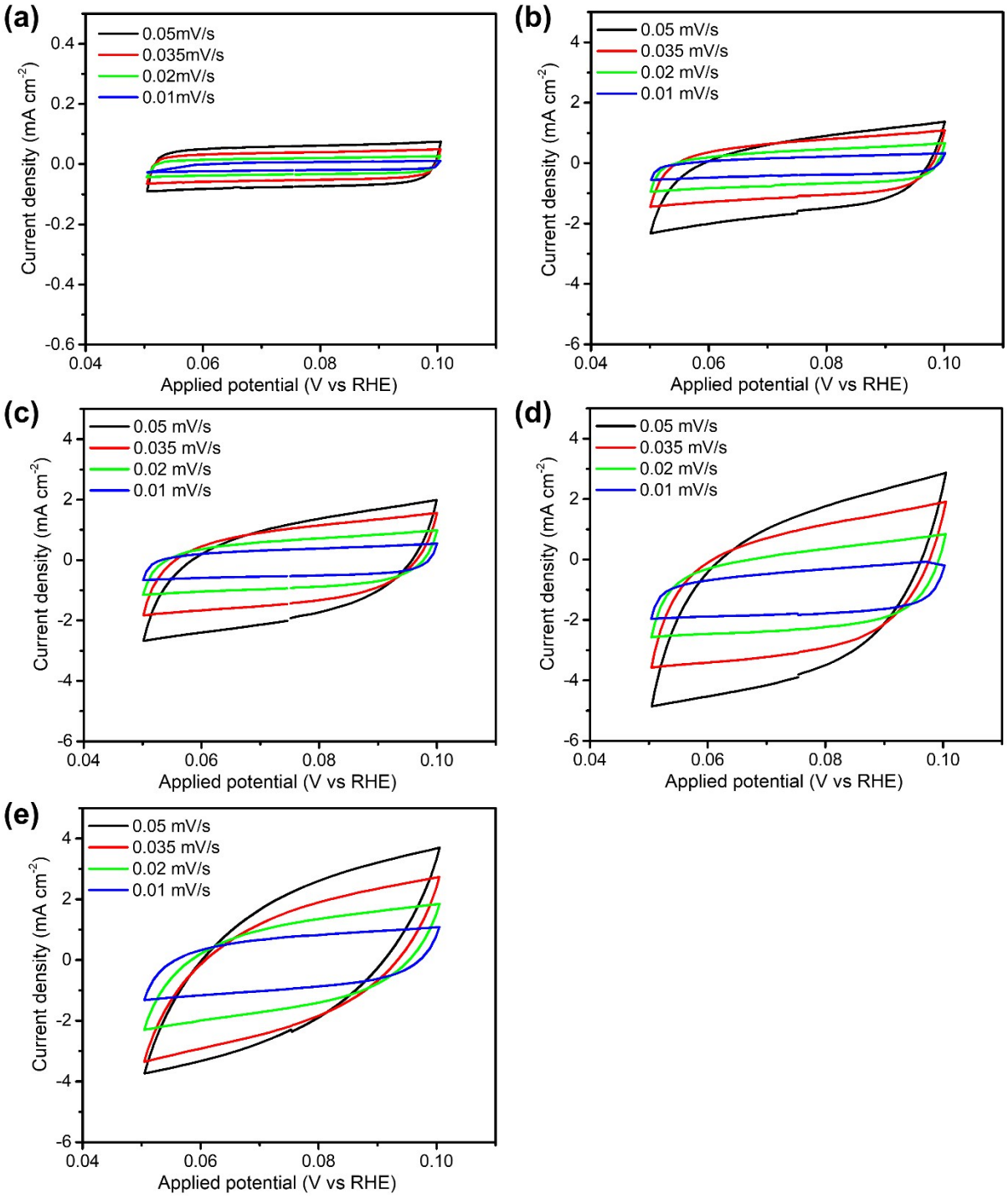

Figure S3. Non-faradaic cyclic voltammograms of (a) dealloyed $Al_{95}Ni_5$ catalyst, (b) dealloyed $Al_{90}Ni_{10}$ catalyst, (c) dealloyed $Al_{85}Ni_{15}$ catalyst, (d) dealloyed $Al_{80}Ni_{20}$ catalyst, and (e) dealloyed $Al_{75}Ni_{25}$ catalyst at different scan rates (0.05, 0.035, 0.02, 0.01 mV s^{-1}) in 1.0 M KOH.

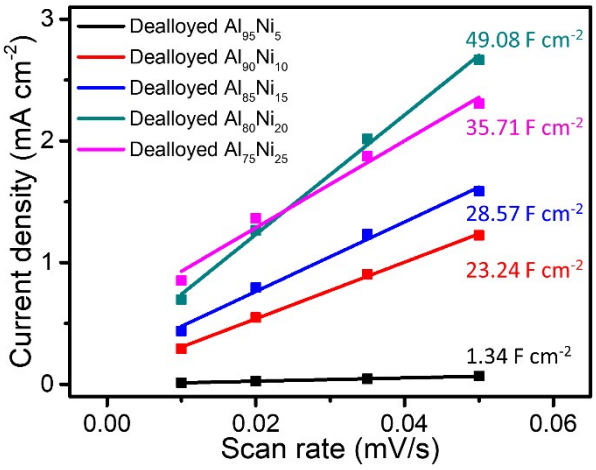

Figure S4. Determination of double layer capacitance of dealloyed Al–Ni catalysts from scan rate dependence of the charging current.

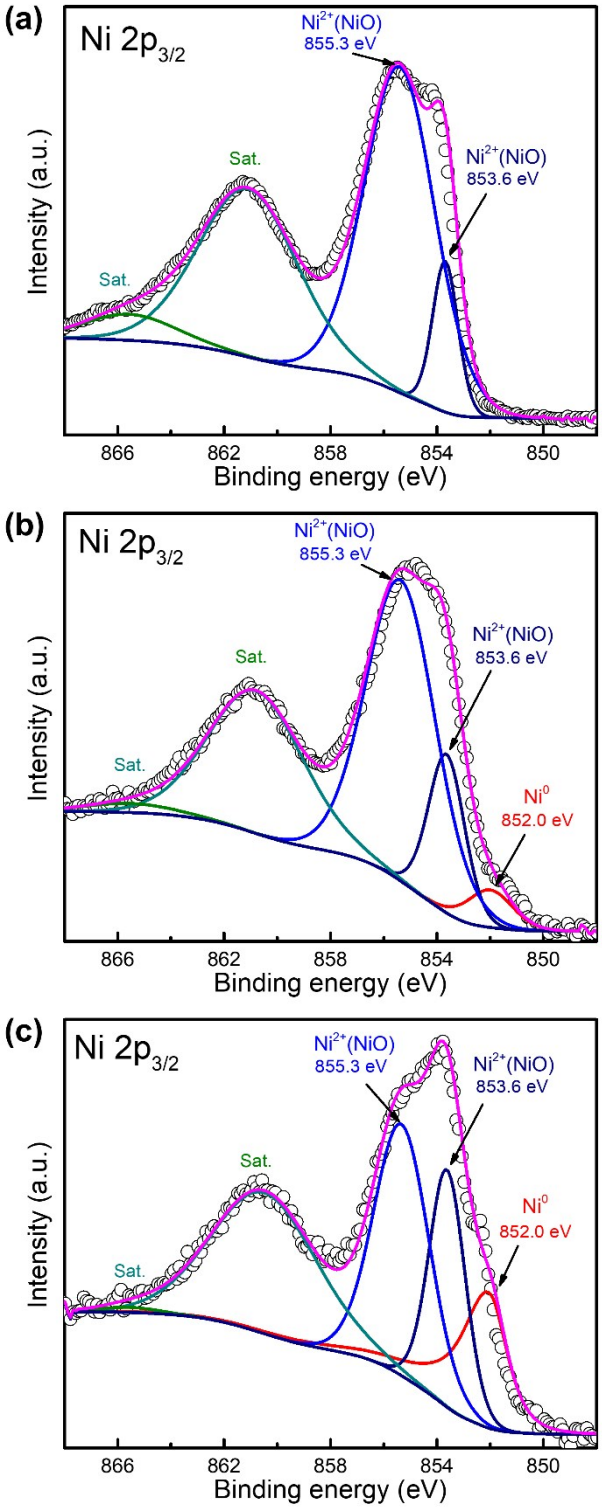

Figure S5. XPS analysis of Ni 2p spectra of dealloyed (a) $Al_{95}Ni_5$, (b) $Al_{90}Ni_{10}$, (c) $Al_{75}Ni_{25}$ catalysts. Similar chemical states of Ni^0 (metal Ni) and Ni^{2+} (NiO) were observed for all samples. The different ratios between multiplet peaks of Ni^{2+} indicate higher proportion of low-coordinated NiO on rod-like structures of dealloyed $Al_{95}Ni_5$ and $Al_{90}Ni_{10}$ catalysts. The

highest activity was observed for dealloyed $Al_{90}Ni_{10}$ catalyst, where both Ni0 sites and rod-like structures coexisted.

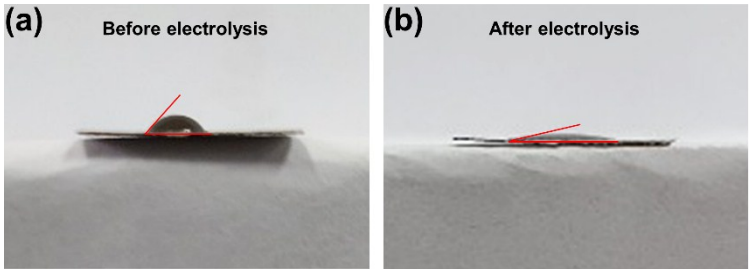

Figure S6. Pictures of contact angle of electrolyte droplet on dealloyed $Al_{90}Ni_{10}$ powder coating electrode (a) before and (b) after the electrolysis for 2h. The contact angle changed from 48° to 13°, showing time-dependent wetting of the electrode, which can be the reason for the increase in current density during the electrolysis.

Table S1. HER activities of dealloyed Al-Ni catalysts and reported Pt-based and NiMo-based catalysts in alkaline media.

Catalysts	η_{10} (mV)	η_{100} (mV)	Tafel (mV dec^{-1})	Ref.
Dealloyed $Al_{95}Ni_5$ catalyst	84	>200	138.7	This work
Dealloyed $Al_{90}Ni_{10}$catalyst	12	83	68.9	This work
Dealloyed $Al_{85}Ni_{15}$catalyst	19	97	74.8	This work
Dealloyed $Al_{80}Ni_{20}$catalyst	46	112	59.4	This work
Dealloyed $Al_{75}Ni_{25}$catalyst	29	126	93.1	This work
Pt plate	50	145	44.2	1
Pt wire	33	120	62	2
Pt/C (20wt%)	24	-	68	3
Pt/C (20wt%)	39	73	34	4
Pt/C (20wt%)	59	-	48.5	5
Pt/C (20wt%)	80	-	63.2	6
NF@Ni–$Ni_{0.2}Mo_{0.8}N$ NRs	15	-	39	7
$MoNi_4/MoO_{3-x}$ NWs	17	52	36	8
Porous NiMo alloy	18	150	36	9
NF@NiMoCo	23	-	34	10
NiMo-NWs/NF	30	-	86	11
O–$NiMoP_2$/Ni	31	-	62.11	12
Ni_4Mo /NF (500 °)	32.2	69.6	37	13
Ni–Mo alloy	35	136	45	14
NiMo-EDA	72	-	89	15
Mo–Ni_2P NW/NF	78	-	109	16
NiMo HNRs/Ti	92	-	76	17
porous NiMoN	109	165	95	18
MoNiNC	110	-	65	19
Ni/MoC_2@NC	130	-	84	20
Mo-NiCo	132.3	-	108	21
Ni–$MoSe_2$	206	-	81	22

Table S2. Tafel slopes of dealloyed Al-Ni catalysts and reported Ni metals for HER in alkaline media.

Catalyst	Tafel ($mVdec^{-1}$)	Ref.
Dealloyed $Al_{95}Ni_5$ catalyst	138.7	This work
Dealloyed $Al_{90}Ni_{10}$catalyst	68.9	This work
Dealloyed $Al_{85}Ni_{15}$catalyst	74.8	This work
Dealloyed $Al_{80}Ni_{20}$catalyst	59.4	This work
Dealloyed $Al_{75}Ni_{25}$catalyst	93.1	This work
Electrodeposited Ni	118	23
Ni metal (in NaOH + NaCl)	130	24
Electrodeposited Ni electrode	115	25
Ni plate	120	26
Ni metal	121	27
Solid Ni	118	28
pure Ni electrode	105	29
Pure Ni metal	~100	30
Polycrystalline Ni	136	31

References

1. Y. Shen, Y. Zhou, D. Wang, X. Wu, J. Li and J. Xi, *Adv. Energy Mater.*, 2018, **8**, 1701759.

2. J. Li, Q. Zhou, Z. Shen, S. Li, J. Pu, C. Zhong, M. Cao, X. Jin, H. Zhang and Y. Wang, *Electrochim. Acta*, 2020, **331**, 135367.

3. S. Zhang, G. Gao, J. Hao, M. Wang, H. Zhu, S. Lu, F. Duan, W. Dong, M. Du and Y. Zhao, ACS Appl. Mater. Interfaces, 2019, 11, 43261-43269.

4. D. Li, B. Zhang, Y. Li, R. Chen, S. Hu and H. Ni, *Electrochem. Commun.*, 2019, **101**, 23-27.

5. T. He, Y. Peng, Q. Li, J. E. Lu, Q. Liu, R. Mercado, Y. Chen, F. Nichols, Y. Zhang and S. Chen, ACS Appl. Mater. Interfaces, 2019, 11, 46912-46919.

6. X. Zhu, X. Zhang, B. Huang, J. Li and E. Wang, J. Mater. Chem. A, 2019, 7, 18304-18310.

7. J. Jia, M. Zhai, J. Lv, B. Zhao, H. Du and J. Zhu, *ACS Appl. Mater. Interfaces*, 2018, **10**, 30400-30408.

8. Y. Y. Chen, Y. Zhang, X. Zhang, T. Tang, H. Luo, S. Niu, Z. H. Dai, L. J. Wan and J. S. Hu, *Adv. Mater.*, 2017, **29**, 1703311.

9. K. Hu, S. Jeong, M. Wakisaka, J.-i. Fujita and Y. Ito, *Metals*, 2018, **8**, 83.

10. K. Hu, M. Wu, S. Hinokuma, T. Ohto, M. Wakisaka, J.-i. Fujita and Y. Ito, *J. Mater. Chem. A*, 2019, **7**, 2156-2164.

11. M. Fang, W. Gao, G. Dong, Z. Xia, S. Yip, Y. Qin, Y. Qu and J. C. Ho, *Nano Energy*, 2016, **27**, 247-254.

12. L. Zhang, X. Wang, X. Zheng, L. Peng, J. Shen, R. Xiang, Z. Deng, L. Li, H. Chen and Z. Wei, *ACS Appl. Energy Mater.*, 2018, **1**, 5482-5489.

13. Z. Xie, Y. Zou, L. Deng and J. Jiang, *Adv. Mater. Interfaces*, 2020, 1901949.

14. Q. Zhang, P. Li, D. Zhou, Z. Chang, Y. Kuang and X. Sun, *Small*, 2017, **13**, 1701648.

15. W. Gao, W. Gou, X. Zhou, J. C. Ho, Y. Ma and Y. Qu, *ACS Appl. Mater. Interfaces*, 2018, **10**, 1728-1733.

16. Y. Sun, L. Hang, Q. Shen, T. Zhang, H. Li, X. Zhang, X. Lyu and Y. Li, *Nanoscale*, 2017, **9**, 16674-16679.

17. J. Tian, N. Cheng, Q. Liu, X. Sun, Y. He and A. M. Asiri, *J. Mater. Chem. A*, 2015, **3**, 20056-20059.

18. Y. Zhang, B. Ouyang, J. Xu, S. Chen, R. S. Rawat and H. J. Fan, *Adv. Energy Mater*, 2016, **6**, 1600221.

19. F. Wang, Y. Sun, Y. He, L. Liu, J. Xu, X. Zhao, G. Yin, L. Zhang, S. Li and Q. Mao,

Nano Energy, 2017, **37**, 1-6.

20. Y. Zhang, X. Xia, X. Cao, B. Zhang, N. H. Tiep, H. He, S. Chen, Y. Huang and H. J. Fan, *Adv. Energy Mater*, 2017, **7**, 1700220.
21. D. Gao, J. Guo, X. Cui, L. Yang, Y. Yang, H. He, P. Xiao and Y. Zhang, *ACS Appl. Mater. Interfaces*, 2017, **9**, 22420-22431.
22. G. Zhao, X. Wang, S. Wang, K. Rui, Y. Chen, H. Yu, J. Ma, S. X. Dou and W. Sun, *Chem. Asian J.*, 2019, **14**, 301-306.
23. R. Bocutti, M. Saeki, A. Florentino, C. Oliveira and A. Angelo, *Int. J. Hydrogen Energy*, 2000, **25**, 1051-1058.
24. B. Tilak, A. Ramamurthy and B. Conway, *Chemical Sciences,* 1986, **97**, 359-393.
25. R. K. Shervedani and A. Lasia, *J. Electrochem. Soc*, 1998, **145**, 2219.
26. T. Burchardt, *Int. J. Hydrogen Energy*, 2000, **25**, 627-634.
27. J. Jakšić, M. Vojnović and N. Krstajić, *Electrochim. Acta*, 2000, **45**, 4151-4158.
28. S. Tanaka, N. Hirose and T. Tanaki, *Int. J. Hydrogen Energy*, 2000, **25**, 481-485.
29. M. Metikoš-Huković and A. Jukić, *Electrochim. acta*, 2000, **45**, 4159-4170.
30. B. Conway, L. Bai and M. Sattar, *Int. J. Hydrogen Energy*, 1987, **12**, 607-621.
31. G. Kreysa, B. Hakansson and P. Ekdunge, *Electrochim. acta*, 1988, **33**, 1351-1357.